ANALYSIS OF DOPPLER-BROADENED PEAK IN THERMAL NEUTRON INDUCED $^{10}B(n,\alpha\gamma)^{7}Li$ REACTION USING HYPERGAM

HEE DONG CHOI*, NAM SUK JUNG and BYUNG GUN PARK
Department of Nuclear Engineering, Seoul National University
San 56-1 Shilim-Dong, Kwanak-Gu, Seoul, 151-744, Korea
*Corresponding author. E-mail : vandegra@plaza.snu.ac.kr

Received July 14, 2008
Accepted for Publication October 16, 2008

The line shape functions for the Doppler-broadened gamma ray spectrum are considered in the $^{10}B(n,\alpha\gamma)^{7}Li$ reaction occurring in a surrounding medium where the excited ^{7}Li nucleus is slowed down and stopped before decay. The phenomenological form of the stopping power was used for the broadening effect. Convolution with the detailed response of a germanium detector is taken into consideration for the simplest case of solely electronic stopping. A numerical study for the analysis of ^{10}B by thermal neutron capture is conducted by performing a parametric search and fitting the measured spectrum in a least-squares approach. In comparison with the previous numerical approach using the same analysis, the computational speed is increased and reliable information concerning the stopping power of the medium is obtained while estimating the uncertainty. Implementation of the routine analysis of ^{10}B is facilitated on a recent version of the gamma ray spectrum analysis package HyperGam.

KEYWORDS : Doppler-Broadened γ-Line Shape Formulae, Kinematic Broadening, Phenomenological Stopping Power, Convoluted Germanium Detector Line Shape, $^{10}B(n,\alpha\gamma)^{7}Li$ Peak Analysis

1. INTRODUCTION

Analysis of the Doppler-broadened (DB) line shape can provide physical information related to a wide range of phenomena. The Doppler shift attenuation method (DSAM) is a well-characterized and useful method to obtain the lifetime of excited nuclei that are produced in a nuclear reaction ([1,2] and the references therein). In the inverted Doppler shift attenuation (IDSA) method, information on the stopping power is obtained for a recoiling ^{7}Li nucleus slowing down in various media by using the reaction of $^{10}B(n,\alpha\gamma)^{7}Li$ as induced by thermal neutrons [3-6]. Experimental efforts are also ongoing to determine the coupling constants in the weak interaction by measuring the decay of a nucleus in a muon capture (μ,ν_{μ}) reaction [7,8]. A recent study investigated the present topic of the DB line shape and its application to the analysis of γ-lines emitted from exotic nuclei near the neutron drip line [9]. Using a high resolution crystal spectrometer, the gamma-ray-induced Doppler effect (GRID), despite being small, was observed for a decaying nucleus recoiling from a cascade gamma ray emission [10]. In a different field and context, the DB line shape obtained from the annihilation of a positron in a medium was shown to be able to probe the momentum distribution of orbital electrons. This technique has been applied to the analysis of materials [11-13]. Therefore, it is clear that the present topic is related to a wide range of applications.

In most of these techniques, an excited nucleus is created in a reaction of $M_2(m_1, m_3)M_4^*$ induced by particle m_1 with laboratory energy E_1. Naturally, many features in the analysis of the Doppler effect are common in these types of experiments. Here, the initial distribution of the recoil particle M_4^* is determined by kinematics and a reaction mechanism. In DSAM measurements, the direction of the recoil particle is confined within a narrow cone of beam direction and hence lead to a Doppler shift of the emitted gamma rays. In other types of measurements such as IDSA and the (μ,ν_{μ}) reaction, the distribution of the recoil particle is omnidirectional or, in a simpler case, isotropic in the laboratory, mainly due to reaction kinematics. The gamma ray emission spectrum in this case is therefore Doppler-broadened in contrast to the Doppler-shifted spectrum in a typical DSAM. This is clearly shown for the two types of reactions by comparing the γ^{-1} factor, which is the ratio of the speed of M_4^* in the center-of-mass (CM) system, to the speed of the CM in the laboratory. This is given by [1]

Table 1. Kinematic Broadening Factor γ^{-1} for Several Types of Reactions

Experimental Type	Reaction (E_x) [reference]	Q_0 [MeV]	E_1 [eV]	γ^{-1}
DSAM	$^{9}Be(d, p)^{10}Be^{*}$(3.37 MeV) [14]	4.590	2.8×10^{6}	0.83
	$^{9}Be(\alpha, n)^{12}C^{*}$(4.43 MeV) [15]	5.704	3.2×10^{6}	0.55
	$^{16}O(^{3}He, p)^{18}F^{*}$(1.70-3.84 MeV) [16]	2.012	3.4×10^{6}	0.57-0.33
IDSA	$^{10}B(n, \alpha)^{7}Li^{*}$(0.478 MeV) [4]	2.792	Thermal (~0.025)	~24000
Muon capture	$^{28}Si(\mu, \nu)^{28}Al^{*}$(2.202 MeV) [17]	101	Moderated (~0.5-1.0)	~570 max.
	$^{16}O(\mu, \nu)^{16}N^{*}$(0.397, 0.298 MeVs) [7]	95		~550 max.

$$\gamma^{-1}=\left[\frac{M_2 m_3}{m_1 M_4^{*}}\left(1+\frac{m_1+M_2}{M_2}\frac{Q}{E_1}\right)\right]^{1/2} \tag{1}$$

where $Q = Q_0 - E_x$, Q_0 is the reaction Q-value for the ground state of M_4, and E_x is the excitation energy of M_4^{*}. In Table 1, the γ^{-1} ratios are shown for a few distinguishing classes of reaction kinematics. The reaction class in the bottom row has a large Q value in comparison to the incoming energy and consequently shows a considerable amount of kinematic broadening. The present study is concerned about the second class of reactions even though the Doppler effect line shape formulae are similar in both reaction classes. For simplification, the following assumptions and approximations are used with respect to reaction and detection.

i) The distribution of the recoil nuclei in the laboratory is isotropic.
ii) The Doppler effect is approximated as a first-order effect in velocity, ß=v/c.
iii) The intrinsic γ-line shape emitted from a stationary nucleus is taken to be infinitely sharp.
iv) The recoil nuclei are stopped by collisions with medium atoms, and the stopping collisions undergo a smooth, continuous process so as not to distort the initial recoil distribution.
v) The gamma rays are measured with a germanium detector of typical resolution.

Under these limiting but realistic assumptions, the DB line shape in this study can be represented by a closed formula with a few parameters. In the most simplified case of stopping, as addressed in an IDSA study of the $^{10}B(n,\alpha\gamma)^{7}Li$ reaction induced by thermal neutron, the emission spectrum is convoluted with the semi-empirical response of a germanium detector, leading to an analytic form. Numerical work has been done for the routine analysis of ^{10}B and the results are shown in this work.

2. REVIEW OF DOPPLER-BROADENED γ-LINE SHAPES

When a gamma ray is emitted at time t from an excited nucleus moving at velocity v(t), the Doppler shifted energy of the gamma ray is given by

$$E_\gamma = E_0\left(1+\frac{v(t)}{c}\cos\theta\right) \tag{2}$$

where E_0 is the energy emitted from a stationary nucleus and θ is the angle between the nucleus velocity and the direction of the emission. By defining a time-independent variable [18],

$$\varepsilon \equiv \frac{E_\gamma - E_0}{E_0 v_0 / c}, \tag{3}$$

where v_0 is the initial velocity of the recoil nucleus, Eq. (2) can be rewritten as

$$\cos\theta = \varepsilon\frac{v_0}{v(t)}. \tag{4}$$

Since the magnitudes of E_0 and v_0 are kinematically fixed, the variable ε in Eq. (3) is a dimensionless scale of the energy E_γ. By considering the recoil nucleus stopping in a medium, v(t) in Eq. (4) is a decreasing function of time and hence, for a given energy ε, $\cos\theta$ is an increasing function of time but is limited to a maximum value of 1. When $\cos\theta = 1$ occurs at time T, $v(t=T) = \varepsilon v_0$ and there is then no further contribution of the DB gamma rays to the given energy interval around ε. The number of gamma rays with energy between ε and ε+dε was studied long ago and it is given by [18]

$$dn(\varepsilon) = \lambda\int_0^T \exp(-\lambda t) I(\cos\theta)\partial_\varepsilon(\cos\theta)\, dt \tag{5}$$

where λ is the gamma decay constant of the excited

nuclear state, $I(\cos\theta)\partial_\varepsilon\cos\theta$ is the intensity of the gamma ray emission at angle θ, and $\partial_\varepsilon\cos\theta$ is a partial derivative with respect to ε at a fixed time t and is equal to $v_0 d\varepsilon / v(t)$. In terms of the recoil nucleus-gamma angular correlation function $W(\theta)$,

$$I(\cos\theta) = \frac{N_0}{2} W(\theta) = \frac{N_0}{2}\left[1 + \sum_{n=2}^{even} a_n P_n(\cos\theta)\right] = \frac{N_0}{2}\sum_{m=0}^{even} b_m \cos^m\theta \quad (6)$$

where N_0 is the total number of gamma emissions, the a_n variables are angular correlation coefficients with n = 2 and 4 generally being sufficient, and the b_m variables are the coefficients of the polynomial in $\cos\theta$ obtained by expanding the Legendre function P_n values. By combining Eqs. (4), (5), and (6), the emission line shape is obtained by

$$\frac{dn(\varepsilon)}{d\varepsilon} = \frac{N_0}{2}\lambda \sum_{m=0}^{even} b_m \varepsilon^m v_0^{m+1} \int_0^T \exp(-\lambda t)\frac{dt}{v^{m+1}(t)} \quad (7)$$

where v(t) is dependent on the slowing down medium. It is therefore obtained by integrating the stopping power equation [9],

$$t = M_4 \int_{v_0}^{v} \frac{dv}{(-dE/dx)} \quad (8)$$

where E is the kinetic energy of the excited nucleus M_4.

A degree of complication exists in different models for describing the energy loss of moving ions in matter. The recently developed and widely-used code SRIM gives the stopping power in tabular data for a wide range of energy and ion-medium combinations [19]. The energy loss theory of Lindhard, Scharff and Schiøtt (LSS) has also been used widely to describe ion stopping in a medium [20]. When either of these stopping powers is used in Eq. (8), however, the integration can only be done numerically. For an empirical approach to the stopping power, the phenomenological expression widely adopted in studies of DSAM is useful for analytic purposes. It is given in the most general form using three parameters [15,16,21], as shown below,

$$-\frac{dE}{dx} = -M_4\frac{dv}{dt} = K_e\frac{v}{v_B} + K_n\frac{v_B}{v} - K_3\left(\frac{v}{v_B}\right)^3 \quad (9)$$

where v_B is the Bohr velocity (=c/137) and the constants K_e, K_n, and K_3 are adjustable parameters. Although the energy loss in Eq. (9) is diverging in the limit of zero velocity, which is inconsistent with the LSS theory and SRIM, Eq. (9) considers a high initial velocity in terms of the K_3 parameter. It is noted that $\tau = 1/\lambda$ is the mean lifetime of the excited state of the nucleus while a characteristic time of slowing down can be defined as $\tau_s = 1/\lambda_s = M_4 v_B/2K$, where K is the combined quantity of K_e, K_n, and K_3, as listed in Appendix A [1]. Using Eq. (9), the time t in Eq. (8) was obtained as a function of speed v in previous studies. This is also discussed in Appendix A [9,21].

To obtain the DB line shape for the most general form of stopping power, the integration in Eq. (7) is performed. Given that analytical integration in Eq. (7) is, however, not easy, the problem was solved by numerical integration in all previous related studies [9,21]. The numerical integration has, however, the drawback of ambiguity in determining the line shape parameters by fitting to an experimental DB spectrum. For example, in a recent study of the ^{28}Al decay fed in a muon capture by ^{28}Si, Fynbo showed that significantly different estimates based on SRIM or the LSS stopping power or the phenomenological estimate by Eq. (9) led to similar line shapes with differences only in detailed aspects [9]. In this study, the general analytical solution for the integration in Eq. (7) is found in terms of special functions. This is listed in Appendix A. The obtained solution is comprised of an Appell function of the first kind [22], where the parameters governing the line shape are λ/λ_s, K_n/K_e, K_3/K_e, and v_0/v_B. From the general analytical solution, it is, however, shown in Appendix A that the line shape is dominated by the magnitude of the ratio of λ/λ_s. This therefore explains the ambiguity of the line shape parameters in a numerical approach for the line shape function as observed when both parameters λ and λ_s are determined by fit to the experimental line shape [9]. Although the Appell function is calculable using an existing mathematical package [23], it is not useful at present to apply to practical problems, as the computation is too slow. Therefore, interest in an exact analytical solution has ebbed, except for theoretical concerns at present.

If the initial recoil velocity, v_0/v_B, of the excited nucleus is not high, the K_3 term in the stopping power can be neglected. If τ is considerably smaller than τ_s, practically all of the excited nuclei decay out before reaching the low velocity region where nuclear stopping dominates. When both of these two conditions are met, the condition of stopping is simply reduced using only the electronic term. The full solutions of Eqs. (7) and (8) in this case are straightforward and were given by Pratt long ago [18]. A practically identical solution with a good illustration of the Doppler-broadening effect and a discussion of the validity of using only the electronic stopping in the $^{10}B(n,\alpha\gamma)^{7}Li$ reaction are given by Neuwirth *et al.* [3,4]. Here, the line shape with no consideration of the angular correlation (m=0 only) is given, as [3,4,18]

$$\frac{dn(\varepsilon)}{d\varepsilon}=\begin{cases}\dfrac{N_0}{2}\dfrac{\lambda/D}{(\lambda/D)-1}\left\{1-|\varepsilon|^{(\lambda/D)-1}\right\}, & \lambda/D\neq 1,\\ \dfrac{N_0}{2}\log\dfrac{1}{|\varepsilon|}, & \lambda/D=1,\end{cases} \tag{10}$$

where the degradation constant D is defined as $D\equiv\lambda_s/2 = K_e/M_4v_B$.

3. ANALYSIS OF MEASURED γ-LINE SHAPES IN THE $^{10}B(n,\alpha\gamma)^{7}Li$ REACTION

The simplest solution given in Eq. (10) is applied in many studies concerning or utilizing $^{10}B(n,\alpha\gamma)^{7}Li$ reaction induced by thermal neutrons. For example, the $^{10}B(n,\alpha\gamma)^{7}Li$ reaction is widely used for the routine detection of boron in samples by thermal neutron activation [24-27]. There are several practical problems in the analysis of a DB boron spectrum. The line shape in Eq. (10) is dependent on the sample medium in terms of the degradation constant D. In addition, there could be gamma rays of energy near 478 keV in the DB peak from the $^{10}B(n,\alpha\gamma)^{7}Li$ reaction with interfering lines originating from impurities or other component elements in the sample. One familiar example is the 472 keV γ-line that is emitted from a neutron capture of ^{23}Na. Therefore, multi-parameter peak fitting is required to resolve the overlapping peaks from the DB peak and to describe the DB peak by the degradation constant D. In the fitting process, a convolution of the emission spectrum with the detector response function is required. Previous studies have solved this problem in terms of numerical integration or convolution or approximate treatment of the line shape [24-29]. These previous methods have limitations in the peak fitting speed, the uncertainty assignment of the line shape parameter especially of the degradation constant D, or in terms of their inaccurate descriptions of the DB line shape. The present study solved the convolution with a detector response by combining analytic functions in a convergent series thereby reducing the computational time required for multi-parameter peak fitting in a routine analysis task. A reliable estimate of the uncertainty on the obtained parameters was also obtained, which is either missing or assigned without details in existing approaches [24-29].

3.1 DB Emission Line Shape

The spectrum of DB gamma rays emitted from $^{7}Li^{*}$ while slowing down in a stopping medium is given by changing the variable ε in Eq. (10) into an explicit parameter [3,4,18,28],

$$g(E)=q\left[1-\left(\frac{|E-E_0|}{E_0v_0/c}\right)^{\frac{\lambda-D}{D}}\right],\quad |E-E_0|\le\Delta E_m \tag{11}$$

where E is the energy of the emitted gamma ray, and q is the height of the spectrum at $E = E_0$, which is related to the number of emitted gamma rays N_0 by $q=\frac{cN_0}{2E_0v_0}\frac{\lambda}{\lambda-D}$. By changing the variables to

$$x\equiv E-E_0,\quad x_m\equiv\frac{E_0v_0}{c}=\Delta E_m,\quad \alpha\equiv\frac{\lambda}{D}-1,$$
$$q_0\equiv\frac{N_0}{2x_m},\ \text{and}\ q=q(\alpha)=q_0\left(1+\frac{1}{\alpha}\right),$$

the emission line shape for the non-zero α is reduced to a suitable form for convolution,

$$g(x)=g^{ND}+g^{D}(x)=q(\alpha)\left[1-\left(\frac{|x|}{x_m}\right)^{\alpha}\right],$$
$$-x_m\le x\le+x_m;\ g(x)=0,\ \text{otherwise x} \tag{12}$$

where x is the amount of Doppler shift, x_m is the maximum amount of Doppler shift, α is a parameter describing the degradation-free effect on the recoil nucleus, and q_0 is the height of the spectrum for emission in a vacuum. Hence, $g^{ND} = q_0$ (= constant) describes the DB spectrum of gamma rays emitted in a vacuum ($\alpha = \infty$), and $g^{D}(x)$ describes the effect of the degradation of $^{7}Li^{*}$ in the stopping medium. The superscripts ND and D denote the medium nondegrading and degrading, respectively. For the case of the $^{10}B(n,\alpha\gamma)^{7}Li$ reaction induced by thermal neutrons, $E_0 = 478$ keV, $v_0/c = 1.6\times10^{-2}$ [4,24], $\Delta E_m = 7.6$ keV, $\lambda = 9.49\pm0.03$ ps^{-1} [30], and typically $0 \le D < 2$-3 ps^{-1} depending on the stopping power of the medium. Hence, α is a positive real number while no terrestrial stopping medium is known to give an α value of less than 1. Cases with α between 0.5 and infinity were considered in the following numerical study.

3.2 Convolution of Detector Response with a DB γ-Line Shape

There are many methods of describing the germanium detector response to a monoenergetic gamma ray. Commonly, the main part of the response is described by a Gaussian function. There are many variants to describe the low-energy tail part of the peak and the shape of the background. In this study, the response functions used for the low-energy tail and the step-background were taken from the code HYPERMET [31]. For a position x relative to the peak position E_0, the peak response is given by

$$f(x)=f_G(x)+f_{ST}(x)=H\exp\left\{-\left(\frac{x}{\delta}\right)^2\right\}+AH\exp\left(\frac{x}{\beta}\right)\frac{1}{2}\operatorname{erfc}\left(\frac{x}{\eta}+\frac{\eta}{2\beta}\right), \tag{13}$$

where $f_G(x)$ describes the Gaussian and $f_{ST}(x)$ describes the short-term tailing effect due to incomplete charge collection and pile-up. By normalizing $f_G(x)$, H is obtained

by $1/\delta\sqrt{\pi}$. For a detailed discussion of the tail response, the Gaussian efficiency function $\varepsilon_G(x)$ for the peak area is introduced, with no tail consideration, by the Gaussian area under a peak divided by the number of gamma rays of mono-energy x, which is emitted from the source. For a simple approach to the DB peak, $\varepsilon_G(x)$ is taken as the center value ε_{G0} (constant) in the domain $-x_m \leq x \leq x_m$. The effect of energy variation in $\varepsilon_G(x)$ on the area is discussed later in this work.

The full detected line shape is obtained by applying a convolution integral between the DB emission spectrum, Eq. (12), and the germanium detector response function, Eq. (13). Previous studies dealt with convolution by applying numerical integration on the Gaussian detector response [24,25,28]. In other cases they used an analytic solution for the restricted case of a non-degraded rectangular spectrum convoluted with a Gaussian response [26,27]. Recent studies consider the numerical convolution of the full detector response functions in Eqs. (13) and (19) for both a degraded spectrum [29] and a non-degraded rectangular spectrum [32].

The convolution integral between the emission spectrum and the detector response functions is given by

$$\begin{aligned} F(x) &= \int_{-\infty}^{+\infty} g(y) * f(x-y)dy \\ &= \int_{-x_m}^{+x_m} g(y) * [f_G(x-y) + f_{ST}(x-y)]dy \\ &= F_G(x) + F_{ST}(x). \end{aligned} \tag{14}$$

The first part of the convolution with the Gaussian function is mainly dominant for the overall DB shape. It is given by a combination of analytic functions and convergent series:

$$\begin{aligned} F_G(x) &= \int_{-x_m}^{+x_m} [g^{ND}(y) + g^{D}(y)] * f_G(x-y)dy \\ &= F_G^{ND}(x) + F_G^{D}(x), \end{aligned}$$

where

$$\begin{aligned} F_G^{ND}(x) &= \int_{-x_m}^{+x_m} g^{ND}(y) * f_G(x-y)dy \\ &= \frac{N_0 \varepsilon_{G0}}{4x_m}\left[\mathrm{erf}\left(\frac{x+x_m}{\delta}\right) - \mathrm{erf}\left(\frac{x-x_m}{\delta}\right)\right], \end{aligned} \tag{15}$$

$$\begin{aligned} F_G^{D}(x) &= \int_{-x_m}^{+x_m} g^{D}(y) * f_G(x-y)dy = \frac{1}{\alpha} F_G^{ND}(x) \\ &- \frac{N_0 \varepsilon_{G0}}{2\delta\sqrt{\pi}}\left(1+\frac{1}{\alpha}\right)\left(\frac{\delta}{x_m}\right)^{\alpha+1} \exp\left(-\frac{x^2}{\delta^2}\right)\Gamma\left(\frac{\alpha}{2}+\frac{1}{2}\right)\sum_{n=0}^{\infty} a_n \left(\frac{x^2}{\delta^2}\right)^n P\left(\frac{\alpha}{2}+\frac{1}{2}+n, \frac{x_m^2}{\delta^2}\right) \end{aligned} \tag{16}$$

with the coefficient a_n values are given by

$$a_n = \frac{\prod_{r=1}^{n}(\alpha+2r-1)}{(2n-1)!!\, n!}, \quad n \geq 1 \quad \text{and} \quad a_0 = 1. \tag{17}$$

Here, $P(\alpha,x)$ is the incomplete gamma function defined as

$$P(\alpha,x) = \frac{1}{\Gamma(\alpha)}\gamma(\alpha,x) = \frac{1}{\Gamma(\alpha)}\int_0^x e^{-t}t^{\alpha-1}dt \quad (\alpha > 0) \tag{18}$$

where $\Gamma(x)$ is the gamma function [33].

In a gamma ray spectrum measured with a modern HPGe detector, the tail term $F_{ST}(x)$ is usually small, which can lead to slight distortion of the low-energy side of a peak. The second integration $F_{ST}(x)$ with the short-term tail function results in greatly complicated expressions comprised of multiple series. As described in section 3.4, it was found that the obtained expression was not only complicated but also that it showed slow convergence of the series in comparison to the alternative method of numerical integration. Therefore, it is not listed in this work, and the integration is substituted by a numerical method.

3.3 Treatment of the Background

The step-background response is due to Compton scattering in the detector (escape peaks) or to Compton scattering into the detector from surrounding materials. Hence, a convolution is required between the DB emission line shape and the step-background response [31] of

$$h_S(x) = \mathrm{SH}\frac{1}{2}\mathrm{erfc}\left(\frac{x}{\sigma}\right). \tag{19}$$

The result is shown in Appendix B. The long-term tailing background function is similar in shape to the short-term tailing function $f_{ST}(x)$ in Eq. (13) but has different values for parameters μ and ν [31]:

$$h_{LT}(x) = \mathrm{TH}\exp\left(\frac{x}{\nu}\right)\frac{1}{2}\mathrm{erfc}\left(\frac{x}{\mu}+\frac{\mu}{2\nu}\right). \tag{20}$$

As T is smaller than H by several orders of magnitude, long-term tailing is not important in reality. Hence, it is neglected in this study.

The continuum background is chosen either by a constant, a first- or a second-order polynomial in x,

$$h_C(x) = a + bx + cx^2 \tag{21}$$

of which the origin is not related to the DB source and therefore, a convolution is not required.

3.4 Numerical Implementation

To check the numerical accuracy and speed of the developed formulae, a calculation of the convolution

integrals in Eqs. (14) and (B-1) was done by numerical integration using the Gaussian quadrature routine 'quadl' in MATLAB [34]. Using the formulae developed in this study with the convergence criteria of 10^{-6} for the sums in Eqs. (16) and (B-1), and using the technique of vectorizing variables, the calculation speed was observed to increase by a factor of approximately 2 compared to that of numerical convolution at the same accuracy. For the case of a short-term tail convolution, the speed was lower due to multiple sums in the obtained formula. Hence, numerical integration is adopted for the convolution of the short-term tail function. Within the adopted numerical accuracy (10^{-6}), both routines give identical results.

Line shapes obtained by the present numerical simulation are shown in Figure 1. Although the magnitude of the short tail is exaggerated compared to that of realistic spectrum measured by a modern HPGe detector, the overall shapes before and after convolution are clearly shown, with parts of the tail and the step-background causing a slight asymmetry in the top region of the DB spectrum.

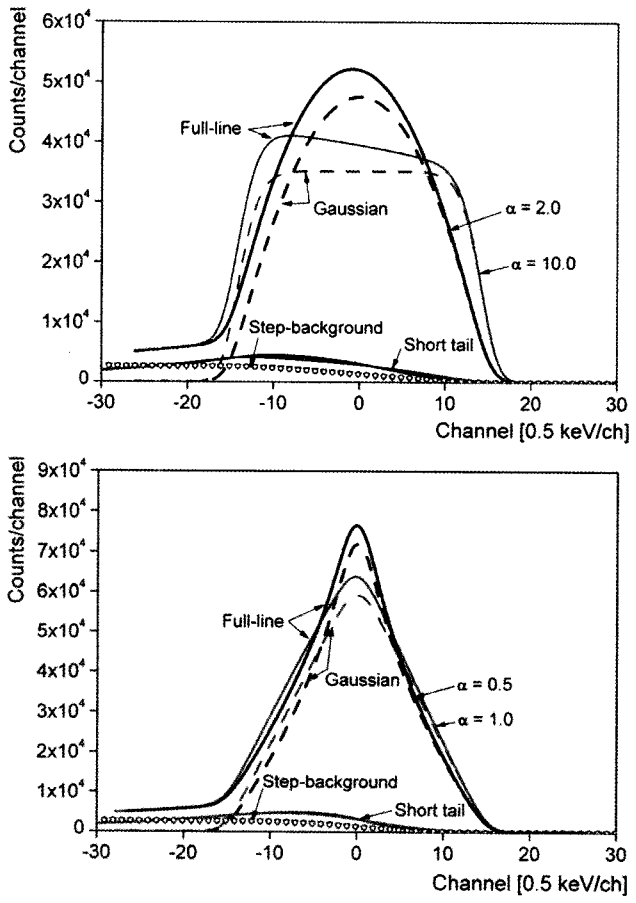

Fig. 1. Full Line Shapes of the DB Spectrum by Including the Convoluted Gaussian, Tail, and Step-Background Responses of a HPGe Detector. The Values Taken are: Gain = 0.5 keV/ch, $N_0 = 9.72 \times 10^5$, $\delta = 2$ ch, A = 0.05, $\eta = \delta$, $\beta = 10\eta$, S = 0.01, and $\sigma = \delta$. The α Values Larger than 1.0 are Considered in the Top Graph: $\alpha = 2.0$ (Black Lines and Filled Symbols) and $\alpha = 10.0$ (Gray Lines and Open Symbols). The α Values Smaller than or Equal to 1.0 are Considered in the Bottom Graph: $\alpha = 0.5$ (Black Lines and Symbols) and $\alpha = 1.0$ (Gray Lines and Open Symbols)

It should be noted that Eq. (15) was derived earlier by assuming no degradation effect and only a Gaussian response in the detector [26]. Due to the fact that the approximations made in previous studies neglected both the degrading effect given in Eq. (12) and the short-term tail response, fitting to realistic data requires x_m as a fit parameter [25-27]. As x_m is a constant determined by the reaction Q-value and γ-transition energy, it is not considered to be a fit parameter but is fixed to 7.6 keV for the $^{10}B(n,\alpha\gamma)^{7}Li$ reaction in the present study.

For a parametric search, the unknown value $N_0\varepsilon_{G0}$ is taken as the single parameter I_G to reduce coding for the developed equations. The integrated area of the DB peak is then given by

$$I = I_G\left\{1+\frac{A\beta}{\delta\sqrt{\pi}}\exp\left(-\frac{\eta^2}{4\beta^2}\right)\right\} \tag{22}$$

using the searched values of I_G, A, δ, η(=δ typically), and ß. When the parameters δ and ß are available from analyses of neighboring peaks, they can be fixed to reduce the number of fit parameters. The full energy peak efficiency $\varepsilon(x)$ is obtained from a reference calibration by defining the peak area comprised of Gaussian and tail parts. In terms of the detector response adopted in HYPERMET, $\varepsilon(x)$ is related to the Gaussian efficiency $\varepsilon_G(x)$ by [31]

$$\varepsilon(x) = \varepsilon_G(x)\left\{1+\frac{A\beta}{\delta\sqrt{\pi}}\exp\left(-\frac{\eta^2}{4\beta^2}\right)\right\} \tag{23}$$

and Eq. (22) is simply reduced to $I = N_0\varepsilon_0$, where ε_0 is the full energy peak efficiency at x = 0. Hence, neglecting the energy dependency of efficiency in the energy region of the DB peak shows that I/ε_0 is equal to the number of gamma rays, N_0, emitted from the source. The area I in Eq. (22) is, however, based on the approximation that the full energy peak efficiency $\varepsilon(x)$ is equal to a constant, ε_0, in the DB peak region. In general, $\varepsilon(x)$ has a slight dependency on x in the region $[-x_m, +x_m]$. Given that it is smooth on x, it could be approximated by a Taylor expansion on x. Considering that the DB peak area is the integration of the incident spectrum g(x) multiplied by $\varepsilon(x)$ and that the spectrum g(x) is an even function of x, only even power terms of x in the expansion of $\varepsilon(x)$ contribute

to the area. As the zero-order term, ε_0, has already been considered, the next high-power term contributing to the area is the second-order correction given by

$$\delta I = I \frac{\alpha+1}{\alpha+3} \frac{\varepsilon_0}{6} \frac{d^2\bar{\varepsilon}}{d\bar{x}^2}\bigg|_{x=0} \tag{24}$$

where $\bar{\varepsilon}(\bar{x})$ is the normalized efficiency function of a dimensionless unit $\bar{x} \equiv x/x_m$. It is defined as

$$\bar{\varepsilon}(\bar{x}) \equiv \frac{\varepsilon(x)}{\varepsilon_0}. \tag{25}$$

Eq. (24) shows that the correction term $\delta I/I$ is proportional to ε_0 and is at most approximately 10^{-3}~10^{-4} for the boron DB peak in a typical germanium detector. Hence, the energy variation of $\varepsilon(x)$ can be neglected in the uncertainty of the fitted area.

When there is no interfering peak in the region of the DB peak, the peak parameters and detector response parameters are determined by least-squares fitting to the measured counts. By denoting the parameters as the vector $\boldsymbol{p}$, the fit function is given by

$$Y = Y(x;\boldsymbol{p}) \equiv F_G(x;\boldsymbol{p}) + F_{ST}(x;\boldsymbol{p}) + H_S(x;\boldsymbol{p}) + h_C(x;\boldsymbol{p}) \tag{26}$$

while up to six Gaussian $G_i(x)$'s with the center of each at $x_{c,\,i}$, the width δ_i taken to be equal to δ, and the height H_i, can be added to $Y(x;\boldsymbol{p})$ when there is interference with the DB peak. The $\boldsymbol{p}$ parameters are determined by minimizing the χ^2-function defined similarly as it is in the code HYPERMET [31]. The covariance matrix of parameters is assigned by obtaining the inverse Hessian matrix, which is given approximately as

$$V_{ij} \cong \left\| \frac{1}{2} \frac{\partial^2 \chi^2}{\partial p_i \partial p_j} \right\|^{-1} \tag{27}$$

where the Hessian matrix is calculated using the final searched parameters [31]. Analytic expressions for the gradient vector and Hessian matrix are derived through tedious algebra. For terms with respect to the short-term tail, numerical derivative and curvature are used instead of an analytic formula due to the complication and slow speed. The uncertainty or the standard deviation of the determined parameter p_i is then given by

$$\sigma(p_i) = \sqrt{\chi_R^2 V_{ii}}. \tag{28}$$

where χ_R^2 is the reduced χ^2, the minimum χ^2 value per degree of freedom of the fit. The uncertainty of DB peak area I is obtained through the propagation of the uncertainties of the relevant parameters with covariances taken into consideration. This is given as

$$\sigma(I) = \sqrt{\chi_R^2 \sum_{i,j} \frac{\partial I}{\partial p_i} V_{ij} \frac{\partial I}{\partial p_j}} \tag{29}$$

with p_i, p_j running on the searched parameters among those appearing in Eq. (22). Developed DB analysis algorithms and routines are incorporated in the HyperGam package recently developed on an interactive MS window platform [35].

3.5 Analysis of DB Peak Measured in the $^{10}B(n, \alpha\gamma)^{7}Li$ Reaction

In Figure 2, the result of an example analysis is shown for the DB peak that is emitted from the $^{10}B(n,\alpha\gamma)^{7}Li$ reaction induced by thermal neutron. The sample is boric acid (H_3BO_3) prepared by drying a diluted aqueous solution. The details of the experimental facility and sample are available in the literature [27,36]. For peak fitting, the Gaussian width parameter δ is fixed by considering the shape-energy dependency obtained from

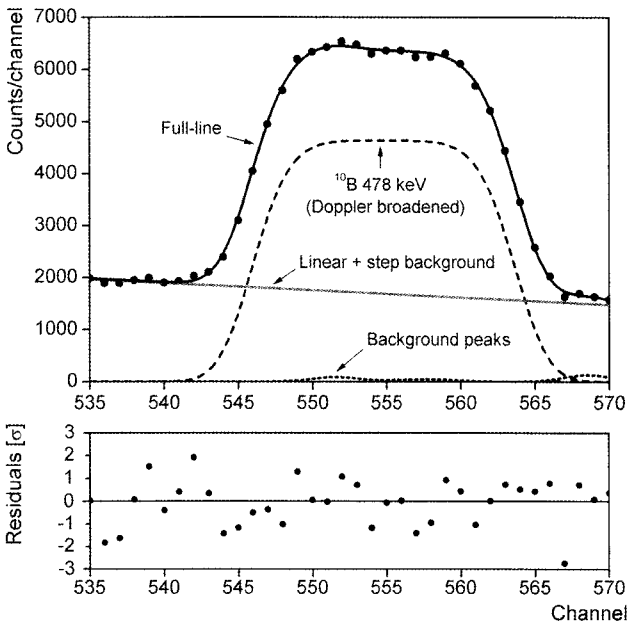

Fig. 2. Analysis of DB Spectrum for Boric Acid (H_3BO_3, B Mass 17.6 μg). The Short Tail and Step-Background Parts are Vanishingly Small but are Included in the Plot. The Determined Values are a DB Peak Area I of 80,300 ± 760 and a Degradation Parameter α of 7.16 ± 0.21

Table 2. The Degradation Constants D (ps^{-1}) Obtained by Various Works on the Slowing Down of a ^{7}Li Ion in Boric Acid (Polycrystalline H_3BO_3, Density 1.435 g/cm^3)

Theoretical		Experimental		
LSS theory [20]	SRIM [19]	Sakai *et al.* [24]	Szentmiklósi *et al.* [29]	This work
1.50 [24]	1.34	1.48	1.29 ± 0.01	1.17 ± 0.03

Table 3. Comparison of the Boron Concentration of a Spinach Sample with the Values of a Previous Work and a Certified Value

Sample	Mass [mg]	Analyzed boron peak count rate [cps]	Boron concentration [μg/g]		
			This work	Previous work [27]	Certified [38]
SRM 1570a spinach	113.2 ± 0.1	9.64 ± 0.27	37.3 ± 1.1	35.2 ± 1.0	37.6 ± 1.0

analyzing the neighboring single energy peaks. The maximum DB width, x_m, of the emitted spectrum is also fixed to the physical value of 7.6 keV with a scale conversion into the channel unit. Hence, parameters are searched for the center and height of the DB peak, degradation parameter α, the heights of the low-energy tail and step-background, and the continuous linear background including those for the interfering Gaussian peaks. The heights of the low-energy tail A and step-background S determined in the fit are very small in this measurement: $A = 1 \times 10^{-3}$, $S = 1 \times 10^{-3}$. The background peaks around the 552, 556, 558 and 568 channels are trivial for obtaining the D-value but improve the fit. The final reduced χ^2 is 1.3. The required time to obtain this result is approximately two minutes. The background peaks are regarded to originate from the decay gamma ray of ^{77}Ge(475 keV) and the background gamma rays of $^{6}Li(n,\gamma)^{7}Li$(478 keV), $^{73}Ge(n,\gamma)^{74}Ge$(478, 482 keV), and $^{72}Ge(n,\gamma)^{73}Ge$(488 keV), respectively. The small background peaks can, however, explain the unsmooth feature on the top of the DB peak. In Table 2, the obtained value of degradation constant D is compared with other reference values which are based on either theories or experiments. The D-value of the SRIM calculation is obtained by fitting a line to the numerical stopping power in the energy region of 90-600 keV. Definite inconsistency is seen between different literature values by considering the associated uncertainties. There are differences in the analysis methods, detector response functions and target material conditions in these experimental works [24,29]. There are also interesting studies to claim the chemical binding effect in the stopping power of compounds, suggesting a deviation from Bragg's rule [5,6,37]. Therefore, a more detailed discussion of this topic requires further research. Figure 3 shows decomposition of the DB boron peak and a strongly interfering gamma ray peak (472 keV) emitted from ^{23}Na capturing neutrons. The target sample is spinach reference material (SRM 1570a) [38]. The same measured spectrum reported in an earlier study [27] is re-analyzed by the current algorithm developed in this study. The new fit resulted in a D-value of 1.56±0.08 ps^{-1} and a boron concentration of 37.3±1.1 μg/g. The results for the boron concentration are summarized in Table 3 for comparison with the value of the previous analysis and a certified value [27,38]. Closer agreement with the certified value was observed in the present analysis.

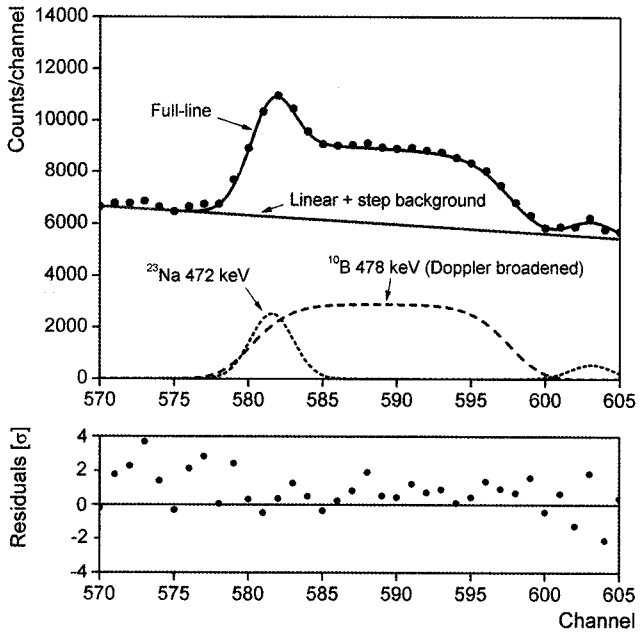

Fig. 3. Decomposition of Boron and Sodium Peaks Measured with a Spinach Sample

4. CONCLUSION

The present work reviewed the DB emission line shape for the most general description of the phenomenological stopping power of the medium in which the excited nucleus recoils and stops. Theoretical line shape formulae are derived and indicate that the dominant parameter governing the DB emission line shape is the ratio λ/λ_s. When both parameters, λ and λ_s, are unknown and hence are determined by a fit to the measured line shape, they can lead to ambiguous result. For an analysis of the ^{10}B DB peak induced by thermal neutron capturing and measured by a germanium detector, the DB emission line shape is greatly simplified and the convolution of the emission line shape with the detector response function is as a result achieved, bring comprised of several analytic functions and a series sum. Based on the analytic functions for the measured line shapes of the ^{10}B DB peak, algorithms for least-square fitting to the measured spectrum are developed and incorporated in HyperGam, a recent interactive software package for gamma ray spectrum analysis. Using the analytic form of line shape functions for the measured spectrum, multiple parameters and their uncertainties relating to the DB peak can be determined reliably at higher speeds by a non-linear least-square fitting method. In summary, the present work has shown that a faster and routine analysis based on closed formulae has become feasible for analysis of a boron DB peak whose shape is strongly dependent on the sample medium. Information on the stopping power of various sample media for recoiling ^{7}Li can also be obtained from the routine analysis. This is suggesting for advanced future works.

APPENDIX

A. The General DB γ-Line Shape

Using Eq. (9), the time t in Eq. (8) was obtained as a function of the speeds v and v_0 previously. It is given by [9,21]

$$t = -\frac{1}{\lambda_s}\log\frac{\phi(v/v_B)}{\phi(v_0/v_B)},$$

$$\phi(x) \equiv \frac{K - K_e + 2K_3x^2}{K + K_e - 2K_3x^2}, \quad K \equiv \sqrt{K_e^2 + 4K_nK_3},$$

$$\text{and } \lambda_s \equiv \frac{2K}{M_4 v_B}. \tag{A-1}$$

When the straightforward inversion of v(t) from Eq. (A-1) is substituted in Eq. (7), the integration is not simple. However, it can be shown that the solution is obtained in terms of a special function, as

$$\frac{1}{\lambda v_B^{m+1}}\left(\frac{2K_3}{K_e - K}\right)^{\frac{m+1}{2}}\left\{F_1\left[p; -\frac{m+1}{2}, \frac{m+1}{2}; p+1; -\phi_0, \frac{K+K_e}{K-K_e}\phi_0\right]\right.$$
$$\left. -\left(\frac{\phi_\varepsilon}{\phi_0}\right)^p F_1\left[p; -\frac{m+1}{2}, \frac{m+1}{2}; p+1; -\phi_\varepsilon, \frac{K+K_e}{K-K_e}\phi_\varepsilon\right]\right\} \tag{A-2}$$

where $p \equiv \lambda/\lambda_s$, $\phi_0 \equiv \phi(v_0/v_B)$, $\phi_\varepsilon \equiv \phi(\varepsilon v_0/v_B)$, and $F_1[a; b,b'; c; x, y]$ is an Appell function of the first kind which is defined for all real or complex values of a, b, b', c, x, and y [22]. One expression of the Appell function $F_1[a; b,b'; c; x, y]$, is given by an infinite series, as

$$F_1[a;b,b';c;x,y] \equiv \sum_{m=0}^{\infty}\sum_{n=0}^{\infty}\frac{(a)_{m+n}(b)_m(b')_n}{(c)_{m+n}\,m!\,n!}x^m y^n \tag{A-3}$$

where $(a)_0 \equiv 1$, $(a)_1 \equiv a$, $(a)_n \equiv a(a+1)(a+2)\ldots(a+n-1)$, ... The calculation of the Appell function in Eq. (A-2) is not trivial and is limited in comparison with the direct numerical integration of Eq. (7). Hence, more work is required for its practical use in parametric fitting as an analysis of line shapes. Nevertheless, it is suitable for checking the analytic properties of the solution. One example calculation of Eq. (A-2) is possible when using a mathematics package [23] and is shown in Figure A-1 for the three cases of λ/λ_s = 0.32, 3.2, and 28.8. The jump at ε = 0 (dn/dε = 0.38) for λ/λ_s = 0.32 is due to the stationary decay described by Eq. (A-4). For λ/λ_s = 3.2 or 28.8, the stationary decay part of the lines is negligible.

Inspection of Eq. (A-2) indicates that for a given value of m, the parameters governing the line shape are

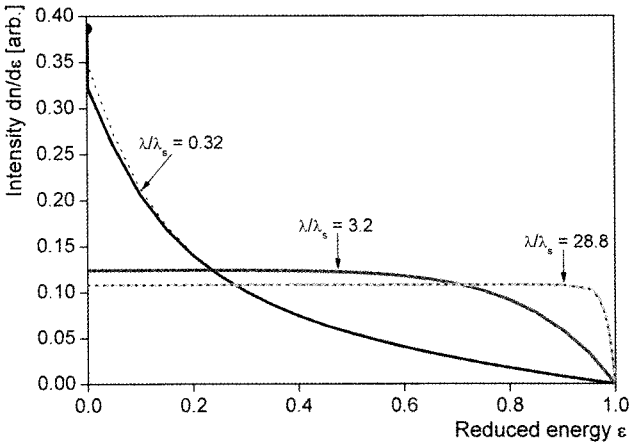

Fig. A-1. Line Shapes for m=0 Calculated by Eq. (A-2) are Shown for the Cases of λ/λ_s = 0.32 (Black), 3.2 (Gray) and 28.8 (Light Gray). The Parameters used for Continuous Lines are K_e = 1, K_n = 0.05, K_3 = 0.03, and v_0/v_B = 2.1. The Dashed Curves used Identical Parameters Except K_e = 1.3 for Each Line

λ/λ_s, K_n/K_e, K_3/K_e, and v_0/v_B. Figure A-1 shows, however, that the line shape is dominated by the magnitude of the ratio of λ/λ_s. As the ratio of λ/λ_s increases, more nuclei decay before slowing down, resulting in a closer rectangular shape. In addition, Figure A-1 shows that even a 30% increase in K_e does not produce a significant difference in the line shape and magnitude once the ratio of λ/λ_s is fixed. This indicates that an analysis of the line shape leads primarily to determining the ratio λ/λ_s. Therefore, use of the correct magnitude of λ or λ_s is required for an unambiguous determination of the other parameter, as it is the ratio λ/λ_s which is mainly determined by fitting the line shape to the measured spectrum.

If the nuclear lifetime $\tau(=1/\lambda)$ is comparable to or larger than the characteristic slowing down time $\tau_s(=1/\lambda_s)$, the fraction of excited nuclei which decay after a full stop is non-negligible. The line shape portion of this stationary decay is described by the delta function $N_0 f_s\,\delta(\varepsilon)$, with

$$f_s = \int_{T_s}^{\infty} \lambda \exp(-\lambda t)dt = \left(\frac{1}{\phi_0}\frac{K-K_e}{K+K_e}\right)^p \qquad \text{(A-4)}$$

where T_s is the time of the full stop and is obtained from Eq. (A-1) with $v(T_s) = 0$. The decay portion in the slowing down is given by Eqs. (7), (A-2) and (A-4) with N_0 replaced with $(1-f_s)N_0$.

When the K_3 term is not important, the first two terms (electronic and nuclear stoppings) in Eq. (9) are used for Eq. (8) and the solution for time t was given by Pratt [18]. It is rewritten here with the present notation as

$$t = -\frac{1}{\lambda_s}\log\frac{\psi(v/v_B)}{\psi(v_0/v_B)}, \qquad \psi(x) = (K_n/K_e) + x^2 \qquad \text{(A-5)}$$

where λ_s is identical to that in Eq. (A-1) with K reduced to K_e. By obtaining v(t), the integration in Eq. (7) can also be performed to give

$$\frac{2}{1-m}\frac{1}{\lambda_s v_0^{m+1}}\frac{1}{\psi_0}\left(\frac{v_0}{v_B}\right)^2\left\{{}_2F_1\left[1,1-p;\frac{3-m}{2};\frac{1}{\psi_0}\left(\frac{v_0}{v_B}\right)^2\right] - \left(\frac{\psi_\varepsilon}{\psi_0}\right)^{p-1}|\varepsilon|^{1-m}\,{}_2F_1\left[1,1-p;\frac{3-m}{2};\frac{1}{\psi_\varepsilon}\left(\frac{\varepsilon v_0}{v_B}\right)^2\right]\right\}$$

(even-m) (A-6)

where $p \equiv \lambda/\lambda_s$, $\psi_0 \equiv \psi(v_0/v_B)$, $\psi_\varepsilon \equiv \psi(\varepsilon v_0/v_B)$, and ${}_2F_1[a, b; c; z]$ is a hypergeometric function also known as the Kummer series or Gauss series [22,33]. A solution for odd-m is relevant only in experiments using a polarized beam [17,18]. It can be obtained from the general solution Eq. (A-2) but it is not directly relevant to this study and is therefore omitted. In some reactions, such as a $^{10}B(n,\alpha\gamma)^7Li$ reaction induced by thermal neutron, simpler treatment of the stopping power is feasible by neglecting both the high-velocity term and nuclear stopping power ($K_3, K_n \to 0$) [3-6]. The corresponding solution for no angular correlation (m=0) can be obtained from Eqs. (7) ~ (9) by a trivial integration [3,4,18] and is given by Eq. (10). Eq. (10) is also obtained from Eq. (A-6) using the properties of hypergeometric functions, which indicates the theoretical consistency of Eqs. (A-2), (A-6) and (10).

B. Convolution of the Step-Background Function

The convolution integral between the source line shape and the step-background in Eq. (19) is given by a combination of analytic functions and convergent series as

$$H_S(x) = \int_{-\infty}^{+\infty} g(y) * h_S(x-y)dy = \int_{-x_m}^{+x_m} g(y) * h_S(x-y)dy = H_S^{ND}(x) + H_S^D(x)$$

$$= \frac{SN_0\varepsilon_{G0}}{4\delta\sqrt{\pi}}\left(1+\frac{1}{\alpha}\right)\left[\frac{x+x_m}{x_m}\operatorname{erfc}\left(\frac{x+x_m}{\sigma}\right) - \frac{x-x_m}{x_m}\operatorname{erfc}\left(\frac{x-x_m}{\sigma}\right) + \right.$$

$$\left. + \frac{\sigma}{x_m\sqrt{\pi}}\left\{\exp\left(-\frac{(x-x_m)^2}{\sigma^2}\right) - \exp\left(-\frac{(x+x_m)^2}{\sigma^2}\right)\right\}\right] -$$

$$- \frac{SN_0\varepsilon_{G0}}{4\delta\sqrt{\pi}}\frac{1}{\alpha}\left[2 + \operatorname{erfc}\left(\frac{x_m+x}{\sigma}\right) - \operatorname{erfc}\left(\frac{x_m-x}{\sigma}\right) - \right.$$

$$\left. - \frac{2}{\sqrt{\pi}}\exp\left(-\frac{x^2}{\sigma^2}\right)\left(\frac{\sigma}{x_m}\right)^{\alpha+1}\left(\frac{x}{\sigma}\right)\Gamma\left(\frac{\alpha+1}{2}\right)\sum_{k=0}^{\infty}c_k\left(\frac{x^2}{\sigma^2}\right)^k P\left(\frac{\alpha}{2}+\frac{3}{2}+k,\frac{x_m^2}{\sigma^2}\right)\right] \qquad \text{(B-1)}$$

where the coefficient c_k is given as

$$c_k = \frac{2^k\prod_{r=0}^{k}(\alpha+2r+1)}{(2k+1)!}, \quad k \geq 0. \qquad \text{(B-2)}$$

REFERENCES

[1] T. K. Alexander and J. S. Forster, *Advances in Nuclear Physics*, Vol. 10, (Eds.) M. Baranger and E. Vogt, Plenum Press, New York (1978).

[2] A. Z. Schwarzschild and E. K. Warburton, "The Measurement of Short Nuclear Lifetimes", *Ann. Rev. Nucl. Sci.*, **18**, 265 (1968).

[3] W. Neuwirth, U. Hauser and E. Kühn, "Energy Loss of Charged Particles in Matter: I. Experimental Method and Velocity Dependence of the Energy Loss of Lithium Ions", *Z. Physik*, **220**, 241 (1969).

[4] U. Hauser, W. Neuwirth, W. Pietsch and K. Richter, "On the Determination of Collision Cross Sections by Nuclear Doppler Shift", *Z. Physik*, **269**, 181 (1974).

[5] W. Neuwirth, W. Pietsch, K. Richter and U. Hauser, "Electronic Stopping Cross Sections of Elements and

Compounds for Swift Lithium Ions", *Z. Physik A*, **275**, 209 (1975).
[6] W. Neuwirth, W. Pietsch, K. Richter and U. Hauser, "On the Invalidity of Bragg's Rule in Stopping Cross Sections of Molecules for Swift Li Ions", *Z. Physik A*, **275**, 215 (1975).
[7] Yu. Shitov, V. Egorov, Ch. Briançon, V. Brudanin, J. Deutsch, T. Filipova, C. Petitjean, R. Prieels, T. Siiskonen, J. Suhonen, Ts. Vylov, V. Wiaux, I. Yutlandov and Sh. Zaparov, "Doppler-broadening of Gamma Rays Following Muon Capture: Search for Scalar Coupling", *Nucl. Phys. A*, **699**, 917 (2002).
[8] B.A. Moftah, E. Gete, D.F. Measday, D.S. Armstrong, J. Bauer, T.P. Gorringe, B.L. Johnson, B. Siebels and S. Stanislaus, "Muon Capture in ^{28}Si and g_p/g_a", *Phys. Lett. B*, **395**, 157 (1997).
[9] H. O. U. Fynbo, "Doppler Broadened γ-lines from Exotic Nuclei", *Nucl. Instr. and Meth. B*, **207**, 275 (2003).
[10] H. G. Börner and J. Jolie, "Sub-picosecond Lifetime Measurements by Gamma Ray Induced Doppler Broadening", *J. Phys. G: Nucl. Part. Phys.*, **19**, 217 (1993).
[11] K. G. Lynn, J. R. MacDonald, R. A. Boie, L. C. Feldman, J. D. Gabbe, M. F. Robbins, E. Bonderup and J. Golovchenko, "Positron-Annihilation Momentum Profiles in Aluminum: Core Contribution and the Independent-Particle Model", *Phys. Rev. Lett.*, **38**, 241 (1977).
[12] M. J. Puska and R. M. Nieminen, "Theory of Positrons in Solids and on Solid Surfaces", *Rev. Mod. Phys.*, **66**, 841 (1994).
[13] P. Asoka-Kumar, M. Alatalo, V. J. Ghosh, A. C. Kruseman, B. Nielsen and K. G. Lynn, "Increased Elemental Specificity of Positron Annihilation Spectra", *Phys. Rev. Lett.*, **77**, 2097 (1996).
[14] E. K. Warburton, D. E. Alburger and D. H. Wilkinson, "Lifetime of the Be^{10} 3.37-MeV Level. I. Experiment", *Phys. Rev.*, **129**, 2180 (1963).
[15] E. K. Warburton, J. W. Olness, K. W. Jones, C. Chasman, R. A. Ristinen and D. H. Wilkinson "Lifetime Determinations for Nuclei A=10, 11, and 12 from Gamma-Ray Doppler Shifts", *Phys. Rev.*, **148**, 1072 (1966).
[16] J. W. Olness and E. K. Warburton, "Studies of F^{18} from the $O^{16}(He^3,p\gamma)F^{18}$ Reaction", *Phys. Rev.*, **151**, 792 (1966).
[17] V. Brudanin, V. Egorov, T. Filipova, A. Kachalkin, V. Kovalenko, A. Salamatin, Yu. Shitov, I. Štekl, S. Vassiliev, V. Vorobel, Ts. Vylov, I. Yutlandov, Sh. Zaparov, J. Deutsch, R. Prieels, L. Grenacs, J. Rak and Ch. Briançon, "Measurement of the Induced Pseudoscalar Form Factor in the Capture of Polarized Muons by Si Nuclei", *Nucl. Phys. A*, **587**, 577 (1995).
[18] T. A. E. C. Pratt, "The Range-Effect in the Gamma-Neutrino Angular Correlation Experiment", *Nucl. Instr. and Meth.* **66**, 351 (1968).
[19] J. F. Ziegler and J. P. Biersack, *The Stopping and Range of Ions in Solids*, Pergamon Press, New York (1985).
[20] J. Lindhard, M. Scharff and H. E. Schiøtt, "Range Concepts and Heavy Ion Ranges (Notes on Atomic Collisions, II)", *Kong. Dansk. Vid. Selsk. Mat.-Fys. Medd.*, **33**, 14 (1963).
[21] E. K. Warburton, J. W. Olness and A. R. Poletti, "Nuclear Structure of Na^{22}. I. Gamma-Ray Correlations and Lifetime Measurements for Levels of E_{ex}<3.1 MeV", *Phys. Rev.*, **160**, 938 (1967).
[22] L. J. Slater, *Generalized Hypergeometric Functions*, Cambridge University Press, Cambridge (1966).
[23] S. Wolfram, *The Mathematica Book*, 5th ed., Wolfram Media (2003).
[24] Y. Sakai, C. Yonezawa, M. Magara, H. Sawahata and Y. Ito, "Measurement and Analysis of the Line Shape of Prompt gamma rays from Recoiling $^{7*}Li$ Produced in the $^{10}B(n, \alpha)^{7}Li$ Reaction", *Nucl. Instr. and Meth. A*, **353**, 699 (1994).
[25] M. Magara and C. Yonezawa, "Decomposition of Prompt Gamma-ray Spectra Including the Doppler-broadened Peak for Boron Determination", *Nucl. Instr. and Meth. A*, **411**, 130 (1998).
[26] S. Baechler, P. Kudejova, J. Jolie, J.-L. Schenker and N. Stritt, "Prompt Gamma-ray Activation Analysis for Determination of Boron in Aqueous Solutions", *Nucl. Instr. and Meth. A*, **488**, 410 (2002).
[27] S. H. Byun, G. M. Sun and H. D. Choi, "Prompt Gamma Activation Analysis of Boron in Reference Materials using Diffracted Polychromatic Neutron Beam", *Nucl. Instr. and Meth. B*, **213**, 535 (2004).
[28] M. K. Kubo and Y. Sakai, "A Simple Derivation of the Formula of the Doppler Broadened 478 keV gamma ray Lineshape from $^{7*}Li$ and Its Analytical Application", *J. Nucl. Radiochem. Sci.*, **1**, 83 (2000).
[29] L. Szentmiklósi, K. Gméling and Zs. Révay, "Fitting the Boron Peak and Resolving Interferences in the 450-490 keV Region of PGAA Spectra", *J. Radioanal. Nucl. Chem.*, **271**, 447 (2007).
[30] R. B. Firestone, V. S. Shirley, C. M. Baglin, S. Y. Frank Chu and J. Zipkin, *Table of Isotopes*, 8th ed., John Wiley & Sons Inc., New York, (1996).
[31] G. W. Phillips and K. W. Marlow, "Automatic Analysis of Gamma-ray Spectra from Germanium Detectors", *Nucl. Instr. and Meth.*, **137**, 525 (1976); G. W. Phillips and K.W. Marlow, *Program HYPERMET for Automatic Analysis of Gamma-Ray Spectra from Germanium Detectors*, NRL Memorandum Report 3198, Naval Research Laboratory, Washington D.C., USA, (1976).
[32] G.M. Sun, C.S. Park and H.D. Choi, "Doppler-broadened boron peak analysis by using a modified spectral decompositon algorithm", *J. Radioanal. Nucl. Chem.*, **278**, 637 (2008).
[33] M. Abramowitz and I. A. Stegun, *Handbook of Mathematical Functions*, Dover Publications, Inc., New York (1970).
[34] W. Gander and W. Gautschi, *Adaptive Quadrature-Revisited, Report 306*, Departement Informatik, ETH Zürich (1998).
[35] C. S. Park, H. D. Choi, G. M. Sun and J. H. Whang, "Status of Developing HPGe gamma ray Spectrum Analysis Code HYPERGAM", *Prog. in Nucl. Energy*, **50**, 389 (2008).
[36] S. H. Byun, G. M. Sun and H.D. Choi, "Development of a Prompt Gamma Activation Analysis Facility Using Diffracted Polychromatic Neutron Beam", *Nucl. Instr. and Meth. A*, **487**, 521 (2002).
[37] Y. Sakai, M. K. Kubo, C. Yonezawa, H. Matsue and M. Jimbo, "Determination of Degradation Constants of Energetic $^{7*}Li$ Ion in Liquid Media Using a Thin Boron Film

on Silicon Wafer", *J. Nucl. Radiochem. Sci.*, **2**, 1 (2001).
[38] R.M. Lindstrom, "Reference Material Certification by Prompt-Gamma Activation Analysis", *Fresenius J. Anal. Chem.*, **360**, 322 (1998).